Article

One-Pot Synthesis of Pd Nanoparticles Supported on Carbide-Derived Carbon for Oxygen Reduction Reaction

Madis Lüsi , Heiki Erikson , Maike Käärik , Helle-Mai Piirsoo , Jaan Aruväli , Arvo Kikas , Vambola Kisand , Jaan Leis , Kaupo Kukli , Kaido Tammeveski *

Posted Date: 7 May 2024

doi: 10.20944/preprints202405.0355.v1

Keywords: oxygen reduction reaction; palladium catalyst; Pd nanoparticles; carbide-derived carbon; electrocatalysis

Article

One-Pot Synthesis of Pd Nanoparticles Supported on Carbide-Derived Carbon for Oxygen Reduction Reaction

Madis Lüsi [1], Heiki Erikson [1], Maike Käärik [1] Helle-Mai Piirsoo [2], Jaan Aruväli [3], Arvo Kikas [2], Vambola Kisand [2], Jaan Leis [1], Kaupo Kukli [2] and Kaido Tammeveski [1,*]

[1] Institute of Chemistry, University of Tartu, Ravila 14a, 50411 Tartu, Estonia
[2] Institute of Physics, University of Tartu, W. Ostwald Str. 1, 50411 Tartu, Estonia
[3] Institute of Ecology and Earth Sciences, University of Tartu, Vanemuise 46, 51014 Tartu, Estonia
* Correspondence: kaido.tammeveski@ut.ee; Tel.: +372 7375168

Abstract: Two methods for Pd nanoparticle synthesis were explored with three different carbide-derived carbon (CDC) support materials of which one was nitrogen-doped. These materials were studied for oxygen reduction reaction (ORR) in 0.1 M KOH solution. The prepared CDC/Pd catalysts were characterized using TEM, XRD and XPS. Using these methods, we can observe the influence of support materials for one-pot synthesis methods as we use the standard citrate method and polyol method with polyvinylpyrrolidone (PVP) as a capping agent. Comparing the two methods N-doping of carbon material resulted in smaller nanoparticles only in the case of citrate synthesis, suggesting that the influence of support is weaker using polyol method. Citrate method on CDC1, which was predominantly microporous led to a higher degree of agglomeration and larger particle formation in comparison to CDC2 and CDC3 supports, which possessed higher degree of mesoporosity. Smaller Pd particle sizes were achieved using citrate and $NaBH_4$ in comparison to the ethylene glycol-PVP method. CDC2 and CDC3 did not show significant difference suggesting that the N-doping did not have much of an influence on the ORR. Highest SA value was observed on CDC1/Pd_Cit, which could be attributed to formation of larger particles and agglomerates.

Keywords: oxygen reduction reaction; palladium catalyst; Pd nanoparticles; carbide-derived carbon; electrocatalysis

1. Introduction

Pd has been researched as a substitute for Pt as the oxygen reduction reaction (ORR) catalyst for the fuel cell cathode side due to its structural similarity and wider availability in the Earth's crust [1–4]. However, the comparison of Pd with Pt is only competitive in alkaline conditions [5–7]. Kim et al. and Arriga et al. noted higher electrocatalytic ORR activity in alkaline media on Pd/graphene in comparison to Pt/graphene [5,7].

There are three routes for improving the utilization of noble metals in the ORR catalyst material. Reduction of loading of noble metal, nano-alloying and improving dispersion and stability through substrate interactions [1–4]. This work focuses on the third category employing carbide-derived carbon (CDC) materials as support for Pd particles.

Pd nanoparticle (PdNP) sizes and shapes are generally limited to a small pool of suitable sizes for the ORR. Jiang and others studied the ORR in alkaline media, while varying Pt particle sizes between 3 to 16.7 nm, with mass activity showing a volcano plot with a maximum around 5 nm and the specific activity (SA) increasing with Pd particle size [8]. The SA effects have also been noted on thin Pd films [9]. Furthermore, different facets of Pd possess varied ORR activity and as such shape-controlled Pd particles dominated by a specific facet exhibit different ORR activity, with the benefiting shape being cuboid [10–16]. The particle shape effect observed in acidic conditions is

 doi:10.20944/preprints202405.0355.v1

conclusive, however in alkaline media Shao and co-workers observed no difference in electrocatalytic activity for their cubic PdNPs if compared to spherical ones [17]. This is also supported by single-crystal study carried out by Hoshi and co-workers on Pd monocrystals in alkaline media as it was shown that the ORR activity increases in the order Pd (110) < Pd (100) < Pd(111) [18], however the differences in the electrocatalytic activity are not as drastic as in $HClO_4$ [19].

Various synthesis methods for PdNP preparation have been studied, which include methods such as microbial and other green methods using plant extracts; however, these methods are rather gimmicky and rarely produce suitable particle size for ORR application [20–26]. In order to obtain any reasonable mass activity for ORR then the noble metal particle size must be below 5 nm, but the number of synthesis methods for achieving these small particles is limited. Methods such as water-in-oil microemulsion require a lot of solvents and are generally not a green approaches for particle synthesis, however, these are suitable to achieve the desired particle size of 5 nm and less [27,28]. Reduction of Pd precursors with alcohol usually leads to larger particles except for anhydrous methanol [29–31], but reduction with ethanol produces particles of 3-12 nm [25]. However, variation of ethanol content with polyvinylalcohol capping agent could lead to better particle size control [32]. There are two good methods of PdNP synthesis based on $NaBH_4$ reduction in the presence of citrate ions and reduction using H_2 at elevated temperature [33]. Ethylene glycol (EG) has been used as a reducing agent for PdNP synthesis, however, typically larger particles are formed; with addition of polyvinylpyrrolidone (PVP) the Pd particles of 4-14 nm have been obtained [34]. However, the addition of hydroxide has been shown to produce suitable Pd particle size [35] and this method was used in this work for comparison.

Since substrate can have an effect on the particle size during the synthesis, one-pot synthesizes can be difficult to reproduce [36–38]. It has been shown that the presence of nitrogen groups on the support can lead to smaller PdNPs in comparison to the non-doped counterpart, which usually leads to better dispersion of particles and improved mass activity of the catalyst. Perini et al. showed using mesoporous carbon a decrease in particle size from 5-6 to 2-3 nm by nitrogen doping the carbon support without the use of surfactants [39]. Similarly, a decrease in particle size was observed by depositing Pd catalyst on graphene and N-doped graphene using plasma synthesis as it drop particle size from 2.8-3.2 to 2.6-2.9 nm [38]. This effect has been also noted using PtM (Pd, Fe, Ni) catalyst, as smaller nanoparticles were observed for all alloys on N-doped carbon black compared to regular undoped carbon black [40]. Another benefit for N-doping has been noted by Perini et al. and Zhang et al. showing increase in stability with N-doped support material [39,41], with contradicting results shown for HOPG in which case N-doping lowered stability [42]. Various materials are used as supports of metal nanoparticles for ORR including covalent organic frameworks and oxides, which can be beneficial for catalyst stability [43,44].

In the present work, two methods for Pd nanoparticle deposition were used. Both methods employed one-pot synthesis procedure using EG as reducing agent with PVP as capping agent and other employing $NaBH_4$ as reducing agent with citrate as capping agent. Three different CDC materials were chosen as support materials of which CDC3 was nitrogen-doped. EG synthesis was only used for CDC2 and CDC3 since these performed best using the citrate method. The prepared catalyst materials were characterized by TEM, XPS, MP-AES and electrochemically using RDE.

2. Materials and Methods

Three carbide-derived carbon (CDC) support materials were employed in this work. The CDC materials were synthesized by chlorine treatment at high temperature. Starting carbides used for the CDC preparation are as follows TiC for CDC1 [45], B_4C for CDC2 [46] and TiCN for CDC3 [47]. Porosities of these materials are provided in Table S1 [46] with corresponding PSD values in Figure S1. These CDC materials were ball-milled according to previous procedure using 4 ml ethanol, 200 mg CDC and 400 rpm for 4 cycles of 30 min and 5 min cool-down period with 0.5 mm balls [48].

CDC/Pd_Cit materials were prepared with simple one pot synthesis. A certain amount of $PdCl_2$ (Sigma Aldrich) was dissolved in water (Millipore, Inc) and HCl (Sigma Aldrich) to which sodium citrate (Sigma Aldrich) and CDC support were added. $PdCl_4^{2-}$ and citrate concentrations were 0.25

 doi:10.20944/preprints202405.0355.v1

mM in which 80 mg of CDC material was dispersed. For all catalysts the nominal 20 wt% Pd loading was used. During stirring 22.3 ml of freshly prepared ice-cold 0.1 M $NaBH_4$ (Aldrich) was added after which the mixture was left to stir for 30 min. After stirring KOH pellets were added to remove citrate and the material was filtered and dried in an oven overnight at 60 °C. Catalysts named CDCx/Pd_Cit with x representing the used CDC.

CDC/Pd_EG materials were synthesized by dissolving 20.9 mg of PVP (MW = 8000) and 20.9 mg of $PdCl_2$ in 25 ml of EG in which 50 mg of CDC had already been dispersed, for acidification 21 µl of kHCl solution was used in the case of CDC2 and kH_2SO_4 in the case of CDC3. After which 7.6 ml KOH in EG was added to reach 0.3 M final concentration. The reaction bath was heated to 190 °C for 1 h. After which EG was evaporated at 200 °C in N_2 atmosphere. Carbon material was re-dispersed in 3 M KOH to remove remnants of PVP and centrifuged 3 times followed by filtering and drying overnight at 60 °C. Pd loading for the catalysts was aimed at 20 wt%. Catalysts are named CDCx/Pd_EG, with x designating the used CDC.

CDC/Pd catalyst materials were dispersed in isopropanol (99.8% Honeywell)/Nafion (5%, Aldrich)/water mixture at ratio of 0.975:0.025:9, of which 6 µl were pipetted onto glassy carbon (GC) disk electrode (d = 5 mm, Origalys, France) rotating at 700 rpm and dried in N_2 flow. For comparison a commercial Pd/C catalyst (20 wt% Premetek, USA) was employed in this work.

For X-ray photoelectron spectroscopy (XPS) measurements the samples were drop-casted onto GC plates and measured using Scienta SES-100 electron energy analyzer using Mg Kα radiation (incident energy 1256.6 eV) from twin anode X-ray source XR3E2. Scanning transmission electron microscopy (STEM) images were obtained by imaging samples drop-casted onto lacey carbon-coated copper grid using a transmission electron microscope Titan Themis 200 (FEI) operating at 200 kV using HAADF and BF detectors. The elemental mapping was done using SuperX (Bruker) energy-dispersive X-ray spectroscopy (EDX) system.

For microwave plasma atomic emission spectroscopy (MP-AES) analysis Anton Par Multiwave PRO microwave digestion system with NXF100 digestion vessel was used to dissolve 10 mg of a catalyst material in 8 ml aqua regia. Metal content of the catalysts was determined using Agilent MP-AES 4210. The crystallographic structure of catalysts was studied by X-ray diffraction (XRD) using a Bruker D8 Advance diffractometer with Cu Kα radiation and 1D-detector (LynxEye XE-T). Profile fitting was done using Bruker TOPAS 6.

Standard three-electrode system was used for electrochemical measurements. The following working, counter and reference electrodes were used: GC electrode covered with catalyst layer, Pt-wire and Pt wire bubbled with continuous H_2 flow and separated from the working electrode compartment with Luggin capillary. Experiments were carried out in 0.1 M KOH solution (p.a., Aldrich) and saturated with Ar (99.999%, Linde Gas), O_2 (99.999%, Linde Gas) or CO (99.97%, Linde Gas). For the rotating disk electrode (RDE) measurements a rotator and speed control unit (OrigaLys ElectroChem SAS) were used, and electrode potential was controlled with PGSTAT128N potentiostat/galvanostat (Metrohm Autolab, The Netherlands). The electrochemistry data was collected using GPES software. Cyclic voltammograms (CVs) were measured between 0.1 and 1.4 V vs RHE at a scan rate of 50 mV s^{-1}. Electrode was conditioned between 0.1 to 0.8 V for 10 cycles at 50 mV s^{-1}. CO-stripping was done at 20 mV s^{-1} between 0.1 and 1 V. The ORR polarization curves were measured between 0.1 and 1.1 V vs RHE at a potential scan rate (v) of 10 mV s^{-1}. The electrode rotation rate (ω) was varied between 360 and 4600 rpm. Electrochemical measurements were made at room temperature (23 ± 1 °C).

3. Results and Discussion

3.1. TEM and MP-AES Studies

Particle sizes were counted from the TEM images and are provided in Table 1 with particle size distribution histograms in Figure S2. The citrate method resulted in smaller Pd particles in comparison to EG/PVP method for both CDC2 and CDC3 substrates. Pd nanoparticles deposited on CDC1 showed similar particle size, however higher degree of agglomeration was observed.

 doi:10.20944/preprints202405.0355.v1

Generally, it has been shown that the presence of nitrogen functional groups in the carbon material leads to smaller PdNPs in the one-pot synthesis methods [39,40,49], however in the case of EG/PVP method used in this work smaller Pd particles were obtained on the CDC2 support, whilst the citrate method gives conventional result. From Figure 1e we can observe that the PdNPs for CDC3/Pd_EG are not spherical when comparing to the CDC2/Pd_EG material (Figure 1d) suggesting that the support has played an important role in shaping these Pd particles. Figure S3 demonstrates N-doping of the CDC3 material, showing well distributed nitrogen species across the entire material.

Pd content was determined by MP-AES (Table 1) and we can observe that for the one-pot synthesis of Pd particles the support material has played a role in Pd metal uptake with microporous CDC1 having lower Pd loading compared to mesoporous CDC2 and CDC3.

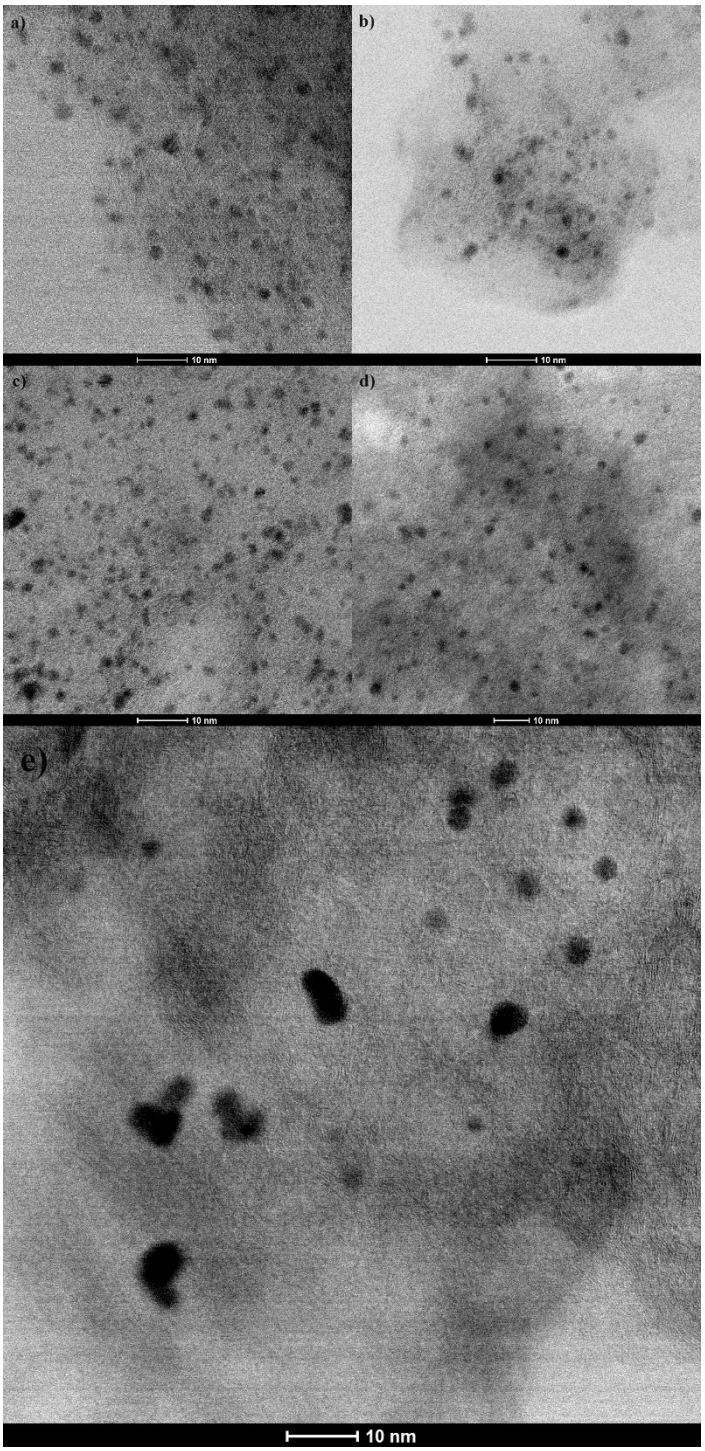

 doi:10.20944/preprints202405.0355.v1

Figure 1. STEM images of CDCx/Pd catalysts: a) CDC1/Pd_Cit, b) CDC2/Pd_Cit, c) CDC3/Pd_Cit, d) CDC2/Pd_EG and e) CDC3/Pd_EG. Scale bar 10 nm.

Table 1. Physical parameters of CDCx/Pd catalysts.

Catalyst	Particle size (nm)	Pd LVol-FWHM (nm)	Lattice parameter (Å)	Pd (wt%)
CDC1/Pd_Cit	2.1 ± 0.5	9.80 ± 0.26 / 1.21 ± 0.01	3.936 / 3.896	15.0
CDC2/Pd_Cit	2.2 ± 0.5	5.57 ± 0.89 / 0.60 ± 0.01	3.898	25.5
CDC3/Pd_Cit	1.8 ± 0.4	2.14 ± 0.08/ 0.50 ± 0.01	3.897	22.6
CDC2/Pd_EG	2.8 ± 0.7	2.09 ± 1.31	3.903	14.8
CDC3/Pd_EG	3.5 ± 1.4	2.18 ± 0.03 / 7.00 ± 1.45*	3.893 / 5.1147*	16.8

* Pd_4S.

3.2. XRD and XPS Analysis

XRD patterns showed the presence of Pd_4S in the case of CDC3/Pd_EG (reflections at 35°, 37.5° and 42.7° can be attributed to Pd_4S). All the samples show loosely connected layered carbon material with some graphitized carbon represented by (002) reflection at 26.4°. Palladium catalyst in the case of citrate synthesis could be separated into two fractions, highly dispersed very small crystallites or amorphous Pd and larger crystallites, which are listed in Table 1. By comparing the CDC materials, we can see that CDC2 has been graphitized to a higher degree compared to the other two CDC materials. Furthermore, with the catalyst material CDC2/Pd_EG we can observe the distance between the loosely connected carbon layers has increased suggesting something pushing these layers apart. Lattice constants (Table 1) observed for catalysts prepared by citrate method are typical of that of Pd at 3.859 Å [50], for one of the phases, however, in the case of CDC1 two observable different sized Pd crystallites were recorded with varied crystallite sizes, CDC2 and CDC3 had very finely dispersed Pd, which made determining lattice constant inaccurate, thus only lattice constant for larger particles are provided. By comparing the XRD patterns and particle sizes counted from TEM images we can observe difference in crystallite size distributions since the XRD method encompasses larger part of the sample the average crystallite size for CDC3/Pd_EG is comparable to that of CDC2/Pd_EG, with N-doped CDC3 providing narrower distribution. The difference in the TEM data could be due to larger Pd_4S particles. Pd3d XPS spectra provided in Figure 3 and the presence of N-doping was also confirmed by XPS (Figure S4, Table S2). Slight difference between the EG and citrate synthesis on CDC2 and CDC3 substrate can be observed in the Pd3d peaks. The observation of the $3d_{3/2}$ peak at ca. 333.4 eV shows that different samples have different ratio of metallic palladium (at 335.4 eV) and Pd^{2+} (336.4 eV [51]). Palladium species and their distribution are provided in Table S3.

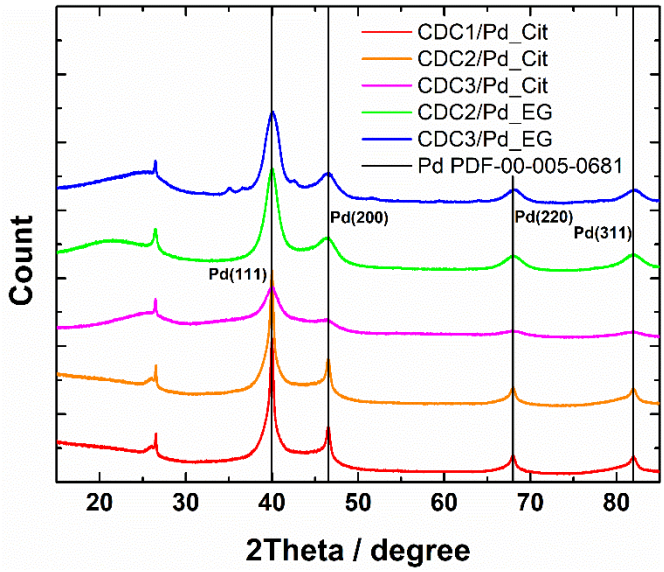

 doi:10.20944/preprints202405.0355.v1

Figure 2. XRD patterns of CDCx/Pd materials.

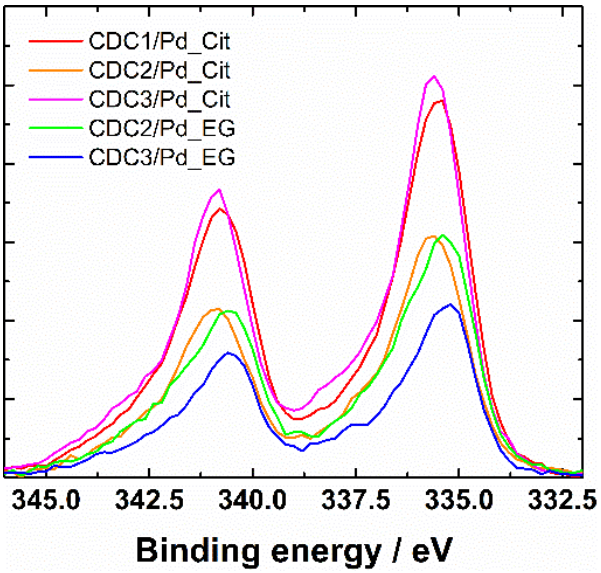

Figure 3. XPS Pd3d spectra of CDCx/Pd materials.

3.3. CV and CO-Stripping Measurements

From CVs we can see that the typical PdO reduction peak is widened by a second peak in the case of citrate synthesis, which can be due to smaller Pd crystallites, as it has been shown that Pd oxide species are generally more stable on smaller particles leading to shift in the peak location [8]. This effect does not appear in the case of EG synthesis, as these smaller crystallites were observed during XRD only in the case of citrate synthesis. The CV profile of the CDCx/Pd_EG catalyst looks typical (Figure 4a) and is comparable to the CV of commercial Pd/C [52]. Furthermore, the change in CVs is provided in Supplementary material. After the ORR measurement we can observe the change in the CV shape in the case of citrate synthesis method (Figures S5-S9), whilst the EG method yields similar CV to the commercial Pd/C. Since the measurements are carried out in alkaline solution and CO-stripping should be able to clean the PdNP surface from citrate if the particles were contaminated [53], it would be observable during the CV studies, however no cleaning effect is observed in the hydrogen desorption area even when CO-stripping was carried out in acidic conditions (Figure S10-S14). However, changing in the peak shape closer to that of the commercial Pd/C is observable, which can be attributed to the low stability of these smaller crystallites (Figure S5-S14). The problem with these CVs is that the typical method of using charge integration under the PdO reduction peak for the electrochemical surface area (ESA) determination is disrupted in the case of materials synthesized using the citrate method. This is further complicated by the shape of the CO-stripping curves, whilst citrate method is giving the typical single peak for CO oxidation profile similar to commercial Pd/C albeit at lower potential (Figure 4b). For EG synthesis method two peaks can be observed, one at around the same potential as for the CDCx/Pd_citrate material and second wider peak stretching to higher potentials. We have previously observed similar CO-stripping behavior for Pd-based catalysts deposited on CDC and other high porous carbon materials and the effect seems to be independent of N-doping [54,55]. One possible explanation for the tailing of the CO-stripping peak can be due to the particle size as tailing of CO-stripping peaks has been previously observed by comparing two commercial Pd/C materials with two different particle size distributions [56]. With the double peak the first peak in case of Pt has been previously attributed to agglomeration [53], another explanation to the first peak is due to catalytically active OH formed on defect sites [57]. However, this further complicates the determination of ESA as the second typically used method for this purpose is unsuitable to compare these catalyst materials. The specific activity (SA) values summarized in Table 2 were obtained using the PdO reduction method for ESA determination in case of EG synthesis and

 doi:10.20944/preprints202405.0355.v1

CO oxidation method for citrate synthesis, as determining ESA based on H_{udp} in alkaline media on Pd electrodes is unreliable.

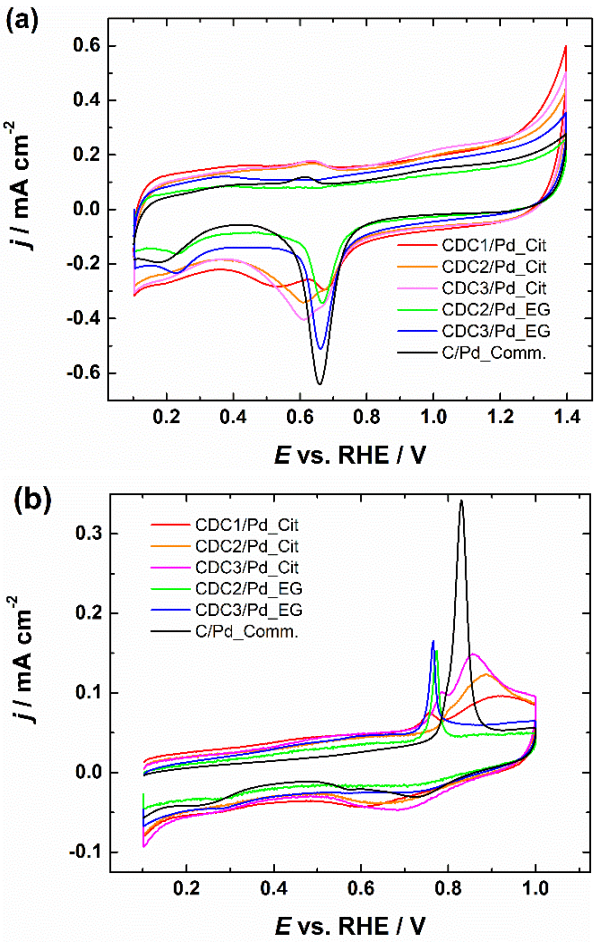

Figure 4. (a) CV curves of CDC/Pd catalysts in Ar-saturated 0.1 M KOH, v = 50 mV s^{-1}. (b) Oxidation of pre-adsorbed CO on CDC/Pd catalysts, v = 20 mV s^{-1}. Current densities are normalized to the geometric area of GC.

Table 2. Kinetic parameters of the prepared Pd-based catalysts for ORR in 0.1 M KOH solution.

Catalyst	ESA (cm^2)	$E_{1/2}$ (V)	Tafel slope (mV)*	SA at 0.9 V (mA cm^{-2})	MA at 0.9 V (A g^{-1})
CDC1/Pd_Cit	0.206	0.834	-61	0.684	341
CDC2/Pd_Cit	0.307	0.844	-66	0.624	289
CDC3/Pd_Cit	0.392	0.858	-61	0.584	414
CDC2/Pd_EG	0.252	0.830	-60	0.512	276
CDC3/Pd_EG	0.356	0.842	-69	0.490	411
C/Pd_Comm	0.589	0.874	-60	0.487	670

*Determined in the potential range of 0.89-0.94 V.

3.3. RDE Measurements

RDE polarization curves for ORR and corresponding Koutecky-Levich plots for are shown in Figures S15-S19, with insets showing the number of electrons transferred (n) calculated by Equation (S1) [58,59], all of the catalysts gave n value ~4 which is typical for Pd catalyst. Comparison of catalyst materials in 0.1 M KOH solution at 1900 rpm can be seen in Figure 5a. The ORR activity in terms of half-wave potentials ($E_{1/2}$) of the citrate synthesis follows order of CDC3/Pd > CDC2/Pd > CDC1/Pd and the Pd catalyst supported on predominantly microporous CDC is performing significantly worse than those deposited on the two other CDC supports with mostly mesopores. Furthermore, CDC3/Pd

 doi:10.20944/preprints202405.0355.v1

material with N-doped support outperforms non-doped counterparts, a similar effect can also be observed for the EG synthesis method as CDC3/Pd is outperforming CDC2/Pd.

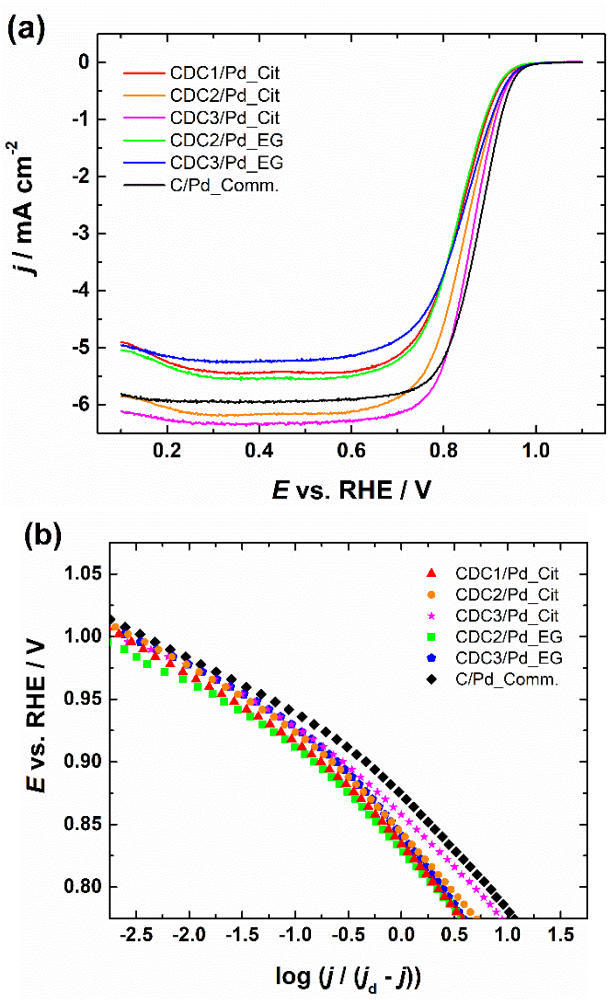

Figure 5. a) Comparison of RDE polarization curves for oxygen reduction in O_2-saturated 0.1 M KOH solution and (b) corresponding Tafel plots, ω = 1900 rpm, v = 10 mV s^{-1}. Current densities are normalized to the geometric area of GC.

Equations (1) and (2) were used to calculate specific (SA) and mass activity (MA):

$$SA = I_k/ESA \quad (1)$$

$$MA = I_k/m, \quad (2)$$

where I_k is the kinetic current at a specific potential, ESA is the surface area of Pd determined by CO-stripping or PdO reduction. m represents Pd mass obtained by MP-AES measurement.

Furthermore, we can see that the citrate synthesis method, which produced smaller PdNPs is showing higher specific activity compared to EG synthesized counterparts as comparing the Pd particle sizes (average particle sizes for CDC2/Pd were 2.8 ± 0.5, 2.2 ± 0.3 nm and for CDC3/Pd 3.4 ± 1.6, 1.8 ± 0.4 nm for EG and citrate synthesis, respectively). However, since CDC2/Pd_EG particles were smaller than those of CDC3/Pd_EG this would suggest that the presence of N-doping has stronger impact on the ORR activity than just decreasing Pd particle size, but this could also be due to the presence of Pd4S. Several researchers have discussed various effects of N-doping on the electrocatalytic activity for ORR. Gracia-Espino et al. suggested that N-doped graphene reduces energy barrier of O2 dissociation [60], however a typical explanation is based on the increase in the number of anchoring sites [61,62]. Comparing the specific activities between the two synthesis

 doi:10.20944/preprints202405.0355.v1

methods is inaccurate as the electrochemical surface area is determined using different method depending on the synthesis, for the CDC2 and CDC3 supported Pd catalysts we can observe rather similar SA values, but comparing to PdNPs deposited on CDC1, which was predominantly microporous, a higher specific activity can be seen. This increase in SA can be attributed to the increased degree of agglomeration and growth of larger Pd crystallites that were seen in the XRD measurements, as it has been shown that larger Pd particles generally possess higher specific activity [8]. Mass activities provided in Table 2 show that different deposition methods resulted in similar MA values, furthermore the effect of sulphur for the CDC3/Pd_EG is negligible. A comparison with literature can be found in Table S4 [8,16,62–69].

Tafel slope values listed in Table 2 were determined in the potential range of 0.89-0.94 V. Tafel slope values are near -60 mV, which is typical for Pd/C catalysts [70–72]. A slightly higher Tafel slope of -69.2 mV was calculated in the case of CDC3/Pd_EG material, which could be due to the presence of Pd_4S as determined by XRD. A similar increase in Tafel slope was observed by Huang et al. in 0.5 M H_2SO_4 [73]. The -60 mV slope is attributed to oxide-covered Pd surface [74] with the rate-determining step for ORR being the transfer of the first electron to the O_2 molecule [70,71]. The increase in Tafel slope has been previously attributed to lowering of the oxide coverage on the Pd nanoparticles [75], which can be beneficial as PdO has been shown to promote $2e^-$ ORR pathway [76].

4. Conclusions

Two approaches were used in this study to prepare Pd nanoparticles on the carbide-derived carbon supports, out of which one was doped with nitrogen. No significant effect from the N-doping was observed for if considering SA, however smaller Pd particles were observed on the N-doped CDC (CDC3/Pd_Cit), leading to improved mass activity. Increase in the specific activity for ORR was noted for CDC1/Pd_Cit, however, this could be attributed to agglomeration and formation of larger Pd particles, which was also observed by XRD. Both of the CDC2 and CDC3 support materials had significant mesoporosity, which seems to facilitate better dispersion of the Pd nanoparticles. N-doped support materials in both cases resulted in higher ESA values in comparison to the non-doped counterpart. Whilst in the case of CDC3/Pd_Cit this could be attributed to smaller average Pd particle size, in the case of CDC3/Pd_EG the particles were larger compared to the CDC2/Pd_EG material, which could suggest a lower degree of agglomeration of Pd nanoparticles in the N-doped CDC material.

Supplementary Materials: The following supporting information can be downloaded at the website of this paper posted on Preprints.org.

Author Contributions: Conceptualization, K.T.; methodology, M.L, H.E, M.K, H-M.P, J.A, A.K, V.K, J.L, K.K and K,T.; validation, M.L, M.K, H-M.P, J.A and A.K; formal analysis, M.L, M.K, H-M.P, J.A and A.K.; investigation, M.L, M.K, H-M.P, J.A and A.K.; resources, V.K, J.L, K.K and K.T.; data curation, M.L.; writing—original draft preparation, M.L.; writing—review and editing, M.L, H.E, M.K, H-M.P, J.A, A.K, V.K, J.L, K.K and K,T.; funding acquisition, V.K, J.L, K.K and K.T. All authors have read and agreed to the published version of the manuscript.

Funding: This research was funded by Estonian Research Council, grant number PRG723, PRG753 and PRG1509. Estonian Ministry of Education and Research, grant number TK210 (Centre of Excellence in Sustainable Green Hydrogen and Energy Technologies).

Data Availability Statement: Dataset available on request from the authors

Acknowledgments: We thank Dr. Peeter Paaver (Institute of Ecology and Earth Sciences of the University of Tartu) for the MP-AES measurements.

Conflicts of Interest: The authors declare no conflicts of interest.

References

1. Antolini, E. Palladium in fuel cell catalysis. *Energy Environ. Sci.* **2009**, *2*, 915-931, doi:10.1039/b820837a.
2. Shao, M. Palladium-based electrocatalysts for hydrogen oxidation and oxygen reduction reactions. *J. Power Sources* **2011**, *196*, 2433-2444, doi:10.1016/j.jpowsour.2010.10.093.

3. Erikson, H.; Sarapuu, A.; Solla-Gullon, J.; Tammeveski, K. Recent progress in oxygen reduction electrocatalysis on Pd-based catalysts. *J. Electroanal. Chem.* **2016**, *780*, 327-336, doi:10.1016/j.jelechem.2016.09.034.
4. Luo, M.; Sun, Y.; Qin, Y.; Li, Y.; Li, C.; Yang, Y.; Xu, N.; Wang, L.; Guo, S. Palladium-based nanoelectrocatalysts for renewable energy generation and conversion. *Mater. Today Nano* **2018**, *1*, 29-40, doi:10.1016/j.mtnano.2018.04.008.
5. Carrera-Cerritos, R.; Baglio, V.; Aricò, A.S.; Ledesma-García, J.; Sgroi, M.F.; Pullini, D.; Pruna, A.J.; Mataix, D.B.; Fuentes-Ramírez, R.; Arriaga, L.G. Improved Pd electro-catalysis for oxygen reduction reaction in direct methanol fuel cell by reduced graphene oxide. *Appl. Catal., B* **2014**, *144*, 554-560, doi:10.1016/j.apcatb.2013.07.057.
6. Jiang, L.; Hsu, A.; Chu, D.; Chen, R. Oxygen Reduction Reaction on Carbon Supported Pt and Pd in Alkaline Solutions. *J. Electrochem. Soc.* **2009**, *156*, B370-B376, doi:10.1149/1.3058586.
7. Seo, M.H.; Choi, S.M.; Kim, H.J.; Kim, W.B. The graphene-supported Pd and Pt catalysts for highly active oxygen reduction reaction in an alkaline condition. *Electrochem. Commun.* **2011**, *13*, 182-185, doi:10.1016/j.elecom.2010.12.008.
8. Jiang, L.; Hsu, A.; Chu, D.; Chen, R. Size-Dependent Activity of Palladium Nanoparticles for Oxygen Electroreduction in Alkaline Solutions. *J. Electrochem. Soc* **2009**, *156*, B643-B649, doi:10.1149/1.3098478.
9. Erikson, H.; Kasikov, A.; Johans, C.; Kontturi, K.; Tammeveski, K.; Sarapuu, A. Oxygen reduction on Nafion-coated thin-film palladium electrodes. *J. Electroanal. Chem.* **2011**, *652*, 1-7, doi:10.1016/j.jelechem.2010.12.021.
10. Erikson, H.; Sarapuu, A.; Tammeveski, K.; Solla-Gullon, J.; Feliu, J.M. Enhanced electrocatalytic activity of cubic Pd nanoparticles towards the oxygen reduction reaction in acid media. *Electrochem. Commun.* **2011**, *13*, 734-737, doi:10.1016/j.elecom.2011.04.024.
11. Erikson, H.; Sarapuu, A.; Alexeyeva, N.; Tammeveski, K.; Solla-Gullon, J.; Feliu, J.M. Electrochemical reduction of oxygen on palladium nanocubes in acid and alkaline solutions. *Electrochim. Acta* **2012**, *59*, 329-335, doi:10.1016/j.electacta.2011.10.074.
12. Lee, C.-L.; Chiou, H.-P. Methanol-tolerant Pd nanocubes for catalyzing oxygen reduction reaction in H2SO4 electrolyte. *Appl. Catal., B* **2012**, *117-118*, 204-211, doi:10.1016/j.apcatb.2012.01.012.
13. Lee, C.-L.; Chiou, H.-P.; Liu, C.-R. Palladium nanocubes enclosed by (100) planes as electrocatalyst for alkaline oxygen electroreduction. *Int. J. Hydrogen Energy* **2012**, *37*, 3993-3997, doi:10.1016/j.ijhydene.2011.11.118.
14. Arjona, N.; Guerra-Balcázar, M.; Ortiz-Frade, L.; Osorio-Monreal, G.; Álvarez-Contreras, L.; Ledesma-García, J.; Arriaga, L.G. Electrocatalytic activity of well-defined and homogeneous cubic-shaped Pd nanoparticles. *J. Mater. Chem. A* **2013**, *1*, 15524-15529, doi:10.1039/C3TA13891G.
15. Huang, K.; Liu, Z.; Lee, C. Truncated palladium nanocubes: Synthesis and the effect of OH- concentration on their catalysis of the alkaline oxygen reduction reaction. *Electrochim. Acta* **2015**, *157*, 78-87, doi:10.1016/j.electacta.2015.01.059.
16. Lusi, M.; Erikson, H.; Sarapuu, A.; Tammeveski, K.; Solla-Gullon, J.; Feliu, J.M. Oxygen reduction reaction on carbon-supported palladium nanocubes in alkaline media. *Electrochem. Commun.* **2016**, *64*, 9-13, doi:10.1016/j.elecom.2015.12.016.
17. Shao, M.H.; Odell, J.; Humbert, M.; Yu, T.Y.; Xia, Y.N. Electrocatalysis on Shape-Controlled Palladium Nanocrystals: Oxygen Reduction Reaction and Formic Acid Oxidation. *J. Phys. Chem. C* **2013**, *117*, 4172-4180, doi:10.1021/jp312859x.
18. Kiguchi, F.; Nakamura, M.; Hoshi, N. Cation Effects on ORR Activity on Low-index Planes of Pd in Alkaline Solution. *Electrochemistry* **2021**, *89*, 145-147, doi:10.5796/electrochemistry.21-00008.
19. Marković, N.M.; Adžić, R.R.; Cahan, B.D.; Yeager, E.B. Structural effects in electrocatalysis: oxygen reduction on platinum low index single−crystal surfaces in perchloric acid solutions. *J. Electroanal. Chem.* **1994**, *377*, doi:10.1016/0022-0728(94)03467-2.
20. Li, C.-J.; Shan, G.-C.; Guo, C.-X.; Ma, R.-G. Design strategies of Pd-based electrocatalysts for efficient oxygen reduction. *Rare Met.* **2023**, *42*, 1778-1799, doi:10.1007/s12598-022-02234-4.
21. Zhang, L.L.; Chang, Q.W.; Chen, H.M.; Shao, M.H. Recent advances in palladium-based electrocatalysts for fuel cell reactions and hydrogen evolution reaction. *Nano Energy* **2016**, *29*, 198-219, doi:10.1016/j.nanoen.2016.02.044.
22. Kumar, G.; Das, S.K.; Nayak, C.; Dey, R.S. Pd "Kills Two Birds with One Stone" for the Synthesis of Catalyst: Dual Active Sites of Pd Triggers the Kinetics of O2 Electrocatalysis. *Small* **2023**, 2307110, doi:10.1002/smll.202307110.
23. Deng, X.; Lao, M.; Zhou, H.; Huang, J.; Li, S.; Liang, Y.; Yin, S.; Xie, Z. Pd Nanoparticles on Carbon Supports as Electrocatalysts for the Oxygen Reduction Reaction. *ACS Appl. Nano Mater.* **2023**, *6*, 20320-20328, doi:10.1021/acsanm.3c04267.

24. Vishnukumar, P.; Vivekanandhan, S.; Muthuramkumar, S. Plant-Mediated Biogenic Synthesis of Palladium Nanoparticles: Recent Trends and Emerging Opportunities. *ChemBioEng Rev.* **2017**, *4*, 18-36, doi:10.1002/cben.201600017.
25. Jukk, K.; Alexeyeva, N.; Johans, C.; Kontturi, K.; Tammeveski, K. Oxygen reduction on Pd nanoparticle/multi-walled carbon nanotube composites. *J. Electroanal. Chem.* **2012**, *666*, 67-75, doi:10.1016/j.jelechem.2011.12.003.
26. Jukk, K.; Alexeyeva, N.; Sarapuu, A.; Ritslaid, P.; Kozlova, J.; Sammelselg, V.; Tammeveski, K. Electroreduction of oxygen on sputter-deposited Pd nanolayers on multi-walled carbon nanotubes. *Int. J. Hydrogen Energy* **2013**, *38*, 3614-3620, doi:10.1016/j.ijhydene.2013.01.062.
27. Wang, C.-C.; Chen, D.-H.; Huang, T.-C. Synthesis of palladium nanoparticles in water-in-oil microemulsions. *Colloids Surf., A* **2001**, *189*, 145-154, doi:10.1016/S0927-7757(01)00576-3.
28. Chen, M.; Feng, Y.-g.; Wang, L.-y.; Zhang, L.; Zhang, J.-Y. Study of palladium nanoparticles prepared from water-in-oil microemulsion. *Colloids Surf., A* **2006**, *281*, 119-124, doi:10.1016/j.colsurfa.2006.02.024.
29. Hirai, H.; Yakura, N. Protecting polymers in suspension of metal nanoparticles. *Polym. Adv. Technol.* **2001**, *12*, 724-733, doi:10.1002/pat.95.
30. Burton, P.D.; Boyle, T.J.; Datye, A.K. Facile, surfactant-free synthesis of Pd nanoparticles for heterogeneous catalysts. *J. Catal.* **2011**, *280*, 145-149, doi:10.1016/j.jcat.2011.03.022.
31. Zhu, Q.-L.; Tsumori, N.; Xu, Q. Immobilizing Extremely Catalytically Active Palladium Nanoparticles to Carbon Nanospheres: A Weakly-Capping Growth Approach. *J. Am. Chem. Soc.* **2015**, *137*, 11743-11748, doi:10.1021/jacs.5b06707.
32. Roy Chowdhury, S.; Sarathi Roy, P.; Bhattacharya, S.K. Green synthesis and characterization of polyvinyl alcohol stabilized palladium nanoparticles: effect of solvent on diameter and catalytic activity. *Adv. Nat. Sci.: Nanosci. Nanotechnol.* **2017**, *8*, 025002, doi:10.1088/2043-6254/aa690e.
33. Lu, L.; Zheng, H.; Li, Y.; Zhou, Y.; Fang, B. Ligand-free synthesis of noble metal nanocatalysts for electrocatalysis. *Chem. Eng. J.* **2023**, *451*, 138668, doi:10.1016/j.cej.2022.138668.
34. Bonet, F.; Delmas, V.; Grugeon, S.; Herrera Urbina, R.; Silvert, P.Y.; Tekaia-Elhsissen, K. Synthesis of monodisperse Au, Pt, Pd, Ru and Ir nanoparticles in ethylene glycol. *Nanostruct. Mater.* **1999**, *11*, 1277-1284, doi:10.1016/S0965-9773(99)00419-5.
35. Chen, L.-J.; Wan, C.-C.; Wang, Y.-Y. Chemical preparation of Pd nanoparticles in room temperature ethylene glycol system and its application to electroless copper deposition. *J. Colloid Interface Sci.* **2006**, *297*, 143-150, doi:10.1016/j.jcis.2005.10.029.
36. Sanij, F.D.; Balakrishnan, P.; Leung, P.; Shah, A.; Su, H.; Xu, Q. Advanced Pd-based nanomaterials for electro-catalytic oxygen reduction in fuel cells: A review. *Int. J. Hydrogen Energy* **2021**, *46*, 14596-14627, doi:10.1016/j.ijhydene.2021.01.185.
37. Lüsi, M.; Erikson, H.; Merisalu, M.; Rähn, M.; Sammelselg, V.; Tammeveski, K. Electrochemical reduction of oxygen in alkaline solution on Pd/C catalysts prepared by electrodeposition on various carbon nanomaterials. *J. Electroanal. Chem.* **2019**, *834*, 223-232, doi:10.1016/j.jelechem.2018.12.061.
38. Lüsi, M.; Erikson, H.; Treshchalov, A.; Rähn, M.; Merisalu, M.; Kikas, A.; Kisand, V.; Sammelselg, V.; Tammeveski, K. Oxygen reduction reaction on Pd nanocatalysts prepared by plasma-assisted synthesis on different carbon nanomaterials. *Nanotechnol.* **2020**, *32*, 035401, doi:10.1088/1361-6528/abbd6f.
39. Perini, L.; Durante, C.; Favaro, M.; Perazzolo, V.; Agnoli, S.; Schneider, O.; Granozzi, G.; Gennaro, A. Metal–Support Interaction in Platinum and Palladium Nanoparticles Loaded on Nitrogen-Doped Mesoporous Carbon for Oxygen Reduction Reaction. *ACS Appl. Mater. Interfaces* **2015**, *7*, 1170-1179, doi:10.1021/am506916y.
40. Yang, H.; Ko, Y.; Lee, W.; Züttel, A.; Kim, W. Nitrogen-doped carbon black supported Pt–M (M = Pd, Fe, Ni) alloy catalysts for oxygen reduction reaction in proton exchange membrane fuel cell. *Mater. Today Energy* **2019**, *13*, 374-381, doi:10.1016/j.mtener.2019.06.007.
41. Zhang, S.Z.; Wang, L.K.; Fang, L.P.; Tian, Y.L.; Tang, Y.; Niu, X.L.; Hao, Y.P.; Li, Z.F. A Facile Method to Prepare Ultrafine Pd Nanoparticles Embedded into N-Doped Porous Carbon Nanosheets as Highly Efficient Electrocatalysts for Oxygen Reduction Reaction. *J. Electrochem. Soc.* **2020**, *167*, doi:10.1149/1945-7111/ab679f.
42. Ju, W.; Favaro, M.; Durante, C.; Perini, L.; Agnoli, S.; Schneider, O.; Stimming, U.; Granozzi, G. Pd Nanoparticles deposited on nitrogen-doped HOPG: New Insights into the Pd-catalyzed Oxygen Reduction Reaction. *Electrochim. Acta* **2014**, *141*, 89-101, doi:10.1016/j.electacta.2014.06.141.
43. Wang, W.; Zhang, L.; Wang, T.; Zhang, Z.; Wang, X.; Cheng, C.; Liu, X. Inner-pore reduction nucleation of palladium nanoparticles in highly conductive wurster-type covalent organic frameworks for efficient oxygen reduction electrocatalysis. *J. Energy Chem.* **2023**, *77*, 543-552, doi:10.1016/j.jechem.2022.11.032.
44. Li, J.; Zhou, H.; Zhuo, H.; Wei, Z.Z.; Zhuang, G.L.; Zhong, X.; Deng, S.W.; Li, X.N.; Wang, J.G. Oxygen vacancies on TiO2 promoted the activity and stability of supported Pd nanoparticles for the oxygen reduction reaction. *J. Mater. Chem. A* **2018**, *6*, 2264-2272, doi:10.1039/c7ta09831f.

45. Käärik, M.; Arulepp, M.; Kook, M.; Mäeorg, U.; Kozlova, J.; Sammelselg, V.; Perkson, A.; Leis, J. Characterisation of steam-treated nanoporous carbide-derived carbon of TiC origin: structure and enhanced electrochemical performance. *J. Porous Mater.* **2018**, *25*, 1057-1070, doi:10.1007/s10934-017-0517-8.
46. Käärik, M.; Arulepp, M.; Käärik, M.; Maran, U.; Leis, J. Characterization and prediction of double-layer capacitance of nanoporous carbon materials using the Quantitative nano-Structure-Property Relationship approach based on experimentally determined porosity descriptors. *Carbon* **2020**, *158*, 494-504, doi:10.1016/j.carbon.2019.11.017.
47. Leis, J.; Arulepp, M.; Käärik, M.; Perkson, A. Method of synthesis of electrocatalytically active porous carbon material for oxygen reduction in low-temperature fuel cells. 2012 WO2013011146A2.
48. Ratso, S.; Zitolo, A.; Käärik, M.; Merisalu, M.; Kikas, A.; Kisand, V.; Rähn, M.; Paiste, P.; Leis, J.; Sammelselg, V.; et al. Non-precious metal cathodes for anion exchange membrane fuel cells from ball-milled iron and nitrogen doped carbide-derived carbons. *Renewable Energy* **2021**, *167*, 800-810, doi:10.1016/j.renene.2020.11.154.
49. Hussain, S.; Erikson, H.; Kongi, N.; Treshchalov, A.; Rahn, M.; Kook, M.; Merisalu, M.; Matisen, L.; Sammelselg, V.; Tammeveski, K. Oxygen Electroreduction on Pt Nanoparticles Deposited on Reduced Graphene Oxide and N-doped Reduced Graphene Oxide Prepared by Plasma-assisted Synthesis in Aqueous Solution. *Chemelectrochem* **2018**, *5*, 2902-2911, doi:10.1002/celc.201800582.
50. Davey, W.P. Precision Measurements of the Lattice Constants of Twelve Common Metals. *Phys. Rev.* **1925**, *25*, 753-761, doi:10.1103/PhysRev.25.753.
51. https://www.xpsfitting.com/2017/10/palladium.html. Available online: (accessed on 01.12.2024).
52. Grden, M.; Lukaszewski, M.; Jerkiewicz, G.; Czerwinski, A. Electrochemical behaviour of palladium electrode: Oxidation, electrodissolution and ionic adsorption. *Electrochim. Acta* **2008**, *53*, 7583-7598, doi:10.1016/j.electacta.2008.05.046.
53. López-Cudero, A.; Solla-Gullón, J.; Herrero, E.; Aldaz, A.; Feliu, J.M. CO electrooxidation on carbon supported platinum nanoparticles: Effect of aggregation. *J. Electroanal. Chem.* **2010**, *644*, 117-126, doi:10.1016/j.jelechem.2009.06.016.
54. Lüsi, M.; Erikson, H.; Sarapuu, A.; Merisalu, M.; Rähn, M.; Treshchalov, A.; Paiste, P.; Käärik, M.; Leis, J.; Sammelselg, V.; et al. Electroreduction of Oxygen on Carbide-Derived Carbon Supported Pd Catalysts. *Chemelectrochem* **2020**, *7*, 546-554, doi:10.1002/celc.201902136.
55. Lüsi, M.; Erikson, H.; Tammeveski, K.; Treshchalov, A.; Kikas, A.; Piirsoo, H.-M.; Kisand, V.; Tamm, A.; Aruväli, J.; Solla-Gullón, J.; et al. Oxygen reduction reaction on Pd nanoparticles supported on novel mesoporous carbon materials. *Electrochim. Acta* **2021**, *394*, 139132, doi:10.1016/j.electacta.2021.139132.
56. Zadick, A.; Dubau, L.; Demirci, U.B.; Chatenet, M. Effects of Pd Nanoparticle Size and Solution Reducer Strength on Pd/C Electrocatalyst Stability in Alkaline Electrolyte. *J. Electrochem. Soc.* **2016**, *163*, F781-F787, doi:10.1149/2.0141608jes.
57. Martins, C.A.; Fernández, P.S.; Troiani, H.E.; Martins, M.E.; Arenillas, A.; Camara, G.A. Agglomeration and Cleaning of Carbon Supported Palladium Nanoparticles in Electrochemical Environment. *Electrocatalysis* **2014**, *5*, 204-212, doi:10.1007/s12678-014-0184-3.
58. Lide, D.R. *CRC handbook of chemistry, and physics*; CRC Press: Boca Raton, 2001.
59. Davis, R.E.; Horvath, G.L.; Tobias, C.W. The solubility and diffusion coefficient of oxygen in potassium hydroxide solutions. *Electrochim. Acta* **1967**, *12*, 287-297, doi:10.1016/0013-4686(67)80007-0.
60. Gracia-Espino, E.; Jia, X.; Wågberg, T. Improved Oxygen Reduction Performance of Pt–Ni Nanoparticles by Adhesion on Nitrogen-Doped Graphene. *J. Phys. Chem. C* **2014**, *118*, 2804-2811, doi:10.1021/jp4101619.
61. Ejaz, A.; Jeon, S. The individual role of pyrrolic, pyridinic and graphitic nitrogen in the growth kinetics of Pd NPs on N-rGO followed by a comprehensive study on ORR. *Int. J. Hydrogen Energy* **2018**, *43*, 5690-5702, doi:10.1016/j.ijhydene.2017.12.184.
62. Wang, X.; Chen, Z.; Chen, S.; Wang, H.; Huang, M. Nitrogen and Oxygen Co-Doping Assisted Synthesis of Highly Dispersed Pd Nanoparticles on Hollow Carbon Spheres as Efficient Electrocatalysts for Oxygen Reduction Reaction. *Chem. Eur. J.* **2020**, *26*, 12589-12595, doi:10.1002/chem.202000901.
63. Chen, Y.; Cai, J.; Li, P.; Zhao, G.; Wang, G.; Jiang, Y.; Chen, J.; Dou, S.X.; Pan, H.; Sun, W. Hexagonal Boron Nitride as a Multifunctional Support for Engineering Efficient Electrocatalysts toward the Oxygen Reduction Reaction. *Nano Lett.* **2020**, *20*, 6807-6814, doi:10.1021/acs.nanolett.0c02782.
64. Wang, M.; Qin, X.; Jiang, K.; Dong, Y.; Shao, M.; Cai, W.-B. Electrocatalytic Activities of Oxygen Reduction Reaction on Pd/C and Pd–B/C Catalysts. *J. Phys. Chem. C* **2017**, *121*, 3416-3423, doi:10.1021/acs.jpcc.6b12026.
65. Yan, W.; Tang, Z.; Li, L.; Wang, L.; Yang, H.; Wang, Q.; Wu, W.; Chen, S. Ultrasmall Palladium Nanoclusters Encapsulated in Porous Carbon Nanosheets for Oxygen Electroreduction in Alkaline Media. *ChemElectroChem* **2017**, *4*, 1349-1355, doi:10.1002/celc.201600885.
66. Khalily, M.A.; Patil, B.; Yilmaz, E.; Uyar, T. Atomic Layer Deposition of Pd Nanoparticles on N-Doped Electrospun Carbon Nanofibers: Optimization of ORR Activity of Pd-Based Nanocatalysts by Tuning Their Nanoparticle Size and Loading. *ChemNanoMat* **2019**, *5*, 1540-1546, doi:10.1002/cnma.201900483.

67. Yang, Y.; Chen, G.; Zeng, R.; Villarino, A.M.; DiSalvo, F.J.; van Dover, R.B.; Abruña, H.D. Combinatorial Studies of Palladium-Based Oxygen Reduction Electrocatalysts for Alkaline Fuel Cells. *J. Am. Chem. Soc.* **2020**, *142*, 3980-3988, doi:10.1021/jacs.9b13400.
68. Si, W.; Yang, Z.; Hu, X.; Lv, Q.; Li, X.; Zhao, F.; He, J.; Huang, C. Preparation of zero valence Pd nanoparticles with ultra-efficient electrocatalytic activity for ORR. *J. Mater. Chem. A* **2021**, *9*, 14507-14514, doi:10.1039/D1TA00788B.
69. Lv, H.; Xu, D.; Sun, L.; Henzie, J.; Suib, S.L.; Yamauchi, Y.; Liu, B. Ternary Palladium–Boron–Phosphorus Alloy Mesoporous Nanospheres for Highly Efficient Electrocatalysis. *ACS Nano* **2019**, *13*, 12052-12061, doi:10.1021/acsnano.9b06339.
70. Vracar, L.M.; Sepa, D.B.; Damjanovic, A. Palladium Electrode in Oxygen-Saturated Aqueous Solutions: Reduction of Oxygen in the Activation-Controlled Region. *J. Electrochem. Soc.* **1986**, *133*, 1835-1839.
71. Vracar, L.M.; Sepa, D.B.; Damjanovic, A. Palladium Electrode in Oxygen-Saturated Aqueous Solutions: Potential Dependent Adsorption of Oxygen Containing Species and Their Effect on Oxygen Reduction. *J. Electrochem. Soc.* **1989**, *136*, 1973-1977, doi: 10.1149/1.2097105, doi:10.1149/1.2109032.
72. Lüsi, M.; Erikson, H.; Merisalu, M.; Kasikov, A.; Matisen, L.; Sammelselg, V.; Tammeveski, K. Oxygen Electroreduction in Alkaline Solution on Pd Coatings Prepared by Galvanic Exchange of Copper. *Electrocatalysis* **2018**, *9*, 400-408, doi:10.1007/s12678-017-0445-z.
73. Huang, Y.; Seo, K.-D.; Park, D.-S.; Park, H.; Shim, Y.-B. Hydrogen Evolution and Oxygen Reduction Reactions in Acidic Media Catalyzed by Pd4S Decorated N/S Doped Carbon Derived from Pd Coordination Polymer. *Small* **2021**, *17*, 2007511, doi:10.1002/smll.202007511.
74. Alvarez, G.F.; Mamlouk, M.; Kumar, S.M.S.; Scott, K. Preparation and characterisation of carbon-supported palladium nanoparticles for oxygen reduction in low temperature PEM fuel cells. *J. Appl. Electrochem.* **2011**, *41*, 925-937, doi:10.1007/s10800-011-0318-8.
75. Shao, M.; Yu, T.; Odell, J.H.; Jin, M.; Xia, Y. Structural dependence of oxygen reduction reaction on palladium nanocrystals. *Chem. Commun.* **2011**, *47*, 6566-6568, doi:10.1039/C1CC11004G.
76. Srejic, I.; Rakocevic, Z.; Nenadovic, M.; Strbac, S. Oxygen reduction on polycrystalline palladium in acid and alkaline solutions: topographical and chemical Pd surface changes. *Electrochim. Acta* **2015**, *169*, 22-31, doi:10.1016/j.electacta.2015.04.032.